IOP PUBLISHING JOURNAL OF NEURAL ENGINEERING
J. Neural Eng. **10** (2013) 000000 (10pp) UNCORRECTED PROOF

Validation of finite element model of transcranial electrical stimulation using scalp potentials: implications for clinical dose

Abhishek Datta[1], **Xiang Zhou**[1], **Yuzhou Su, Lucas C Parra and Marom Bikson**[2]

Neural Engineering Laboratory, Department of Biomedical Engineering, The City College of New York of City University of New York, NY 10031, USA

E-mail: bikson@ccny.cuny.edu

Received 19 May 2012
Accepted for publication 9 April 2013
Published DD MM 2013
Online at stacks.iop.org/JNE/10/000000

Abstract
Objective. During transcranial electrical stimulation, current passage across the scalp generates voltage across the scalp surface. The goal was to characterize these scalp voltages for the purpose of validating subject-specific finite element method (FEM) models of current flow. *Approach*. Using a recording electrode array, we mapped skin voltages resulting from low-intensity transcranial electrical stimulation. These voltage recordings were used to compare the predictions obtained from the high-resolution model based on the subject undergoing transcranial stimulation. *Main results*. Each of the four stimulation electrode configurations tested, resulted in a distinct distribution of scalp voltages; these spatial maps were linear with applied current amplitude (0.1 to 1 mA) over low frequencies (1 to 10 Hz). The FEM model accurately predicted the distinct voltage distributions and correlated the induced scalp voltages with current flow through cortex. *Significance*. Our results provide the first direct model validation for these subject-specific modeling approaches. In addition, the monitoring of scalp voltages may be used to verify electrode placement to increase transcranial electrical stimulation safety and reproducibility.

Q1 (Some figures may appear in colour only in the online journal)

Introduction

Low-intensity transcranial electrical stimulation (TES) encompasses a range of clinical and experimental protocols which apply current through scalp electrodes for the purpose of modulating brain function (Calancie *et al* 1998, Fregni *et al* 2005, Lisanby 2007, Nitsche and Paulus 2000, Rothwell *et al* 1994, Schroeder and Barr 2001), including transcranial direct current stimulation (tDCS), transcranial pulsed current stimulation (Datta *et al* 2012a), transcranial alternating current stimulation (tACS) and cranial electrotherapy stimulation. In all cases, applied current first distributes throughout the scalp, and then passes across the skull and cerebro-spinal fluid (CSF), before eventually entering the brain (Datta *et al* 2009). The goal of this study was to characterize scalp voltages generated during low-intensity TES for the purpose of validating models of current flow, as well as to evaluate how these voltages can be used to understand and refine TES protocols.

For rational and safe therapy, it is paramount to understand the current distribution in the brain during TES. Analytical models using spheres predict brain current flow and have been experimentally validated using a half-skull tank model (Rush and Driscoll 1968). Over the years, analytical approaches have continued to be used (Ferdjallah *et al* 1996,

[1] These authors contributed equally to this work.
[2] Author to whom any correspondence should be addressed.

Saypol *et al* 1991, Stecker 2005). More recently, spherical-based models (Datta *et al* 2008, Miranda *et al* 2006) using finite element methods (FEM) and increasingly detailed gyri-sulci precise magnetic resonance imaging (MRI)-derived high resolution models have been developed (Datta *et al* 2009, Salvador *et al* 2010). However, analytical/spherical-based approaches, animal models, resected skulls, and synthetic phantoms are of limited use because of the critical importance of anatomy and material properties. In 1975, a study measured current flow intra-cortically due to dc stimulation in patients undergoing presurgical evaluation for epilepsy (Dymond *et al* 1975). This study remains the only one with direct measurement in humans to-date. We have recently used patient-specific models to retrospectively analyze the success of a given electrode montage (Datta *et al* 2011) and compared model predictions with patterns of activation revealed by functional MRI (fMRI) signal (Halko *et al* 2011, Antal *et al* 2012). As MRI-derived FEM models may be used to characterize clinical electrotherapies (Bikson *et al* 2010, Dasilva *et al* 2012, Im *et al* 2012, Mendonca *et al* 2011, Parazzini *et al* 2011, Sadleir *et al* 2010) as well as design new electrode montages (Borckardt *et al* 2012), it is important to experimentally validate the accuracy of these FEM models. Toward this end, though it is not evidently safe to record clinically with invasive intra-cortical electrodes, it is practical to record surface potentials on the scalp that are generated during transcranial stimulation.

We propose that during TES, electrode configuration and anatomy determine current distribution through the scalp, which is reflected in scalp voltage maps, and which ultimately determine the distribution of the underlying brain current flow. Here we mapped scalp voltages and validated the accuracy of a subject-specific FEM model of TES. To precisely control the applied electrical stimulation, we used specialized high-definition (HD) stimulation electrodes (Minhas *et al* 2010), rather than large 'sponge' electrodes. We first explored linearity of induced scalp voltages over a very low intensity (0.1–1 mA) and frequency range (1 to 10 Hz) using one montage. We then tested four illustrative montages (including the one used for linearity) and show that each of these montages result in distinct scalp surface voltages and spatial profiles that are predicted by our high-resolution FEM simulations, thus providing needed validation for these broadly used models (Bikson and Datta 2012). Finally, the spatial linear summation of two independent sources was compared to a multiple source. Moreover, we illustrate how these induced surface potentials provide insight into the distribution of brain current flow, and can thus be used in the design of effective and specific transcranial stimulation electrode montages. Lastly, we discuss how online voltage measurement can be used to increase the safety profile of TES.

Methods

Imaging and computational methods

MRI acquisition and segmentation. MRI of brain was performed on a 34 year old male with no neurological pathologies using a 3T Philips Achieva scanner (Philips Medical Systems, Best, Netherlands). Three-dimensional spoiled gradient image (SPGR) was acquired with TE/TR = 3 ms/6.6 ms, flip angle = 8, acquisition matrix = 256 × 256 × 190, and voxel size = 1 × 1 × 1 mm.

Automatic segmentation was performed by FSL's Brain Extraction Tool (Smith 2002) and FSL's Automated Segmentation Toolbox (Zhang *et al* 2001). The head was segmented into five compartments: scalp, skull, CSF, gray and white matter. Using a combination of segmentation and manual editing tools (Simpleware Ltd, Exeter, UK), errors in the automated masks were corrected and the data was further segmented into tissue types representing the eye, muscle, and air (Soterix Medical, NY).

Following the 10–10 international system (conventionally used in EEG), 64 electrodes and gel were automatically positioned on the segmented scalp surface using an in-house custom MATLAB script (Dmochowski *et al* 2011). All simulated electrodes were ∼2 mm thick with a diameter of ∼11 mm separated from the scalp by a 1–2 mm thick layer of gel (figure 1).

Stimulating electrode configurations. Two or six electrodes were energized as stimulating electrodes according to one of following four electrode configurations tested (see below); the remaining electrodes were not activated.

(1) 'Proximal-bipole': stimulation with two adjacent EEG locations—C2 and Cz.
(2) 'Distant-bipole': stimulation with two distant EEG locations—AF4 and Cz.
(3) '4 × 1 concentric-ring': stimulation with electrodes at C3, C4, Fz, Pz enclosing an electrode at Cz.
(4) 'Ring + bipole': stimulation combining the distant-bipole and the 4 × 1 concentric-ring configurations with a shared common electrode of Cz.

FEM analysis. The tissue and the electrode/gel masks were adaptively meshed (Simpleware) and exported into COMSOL Multiphysics (Comsol 3.5a, Burlington, MA) for computation of current flow in the head. The classical Laplace equation for volume conduction was solved with a linear iterative system solver of conjugate gradients (relative tolerance = 1×10^{-6}). The following isotropic direct current electrical conductivities in (S m^{-1}) were assigned: scalp (0.465); skull (0.01); CSF (1.65); gray matter (0.276); white matter (0.126); eye (0.4); muscle (0.334); air (1×10^{-15}); electrode (5.8×10^{7}); gel (0.3) (Datta *et al* 2011, Wagner *et al* 2007). The model comprised >10 million elements with >15 million degrees of freedom.

For the bipolar configurations, current density corresponding to 1 mA total current was applied at the anode electrode. For the 4 × 1-ring configuration, each of the anode electrode(s) injected 0.25 mA current resulting in 1 mA total injected anodal current. For the ring + bipole configuration, 1 mA was applied at the AF4 anode electrode and 0.25 mA each was applied at C3, C4, Fz, Pz. Ground boundary condition

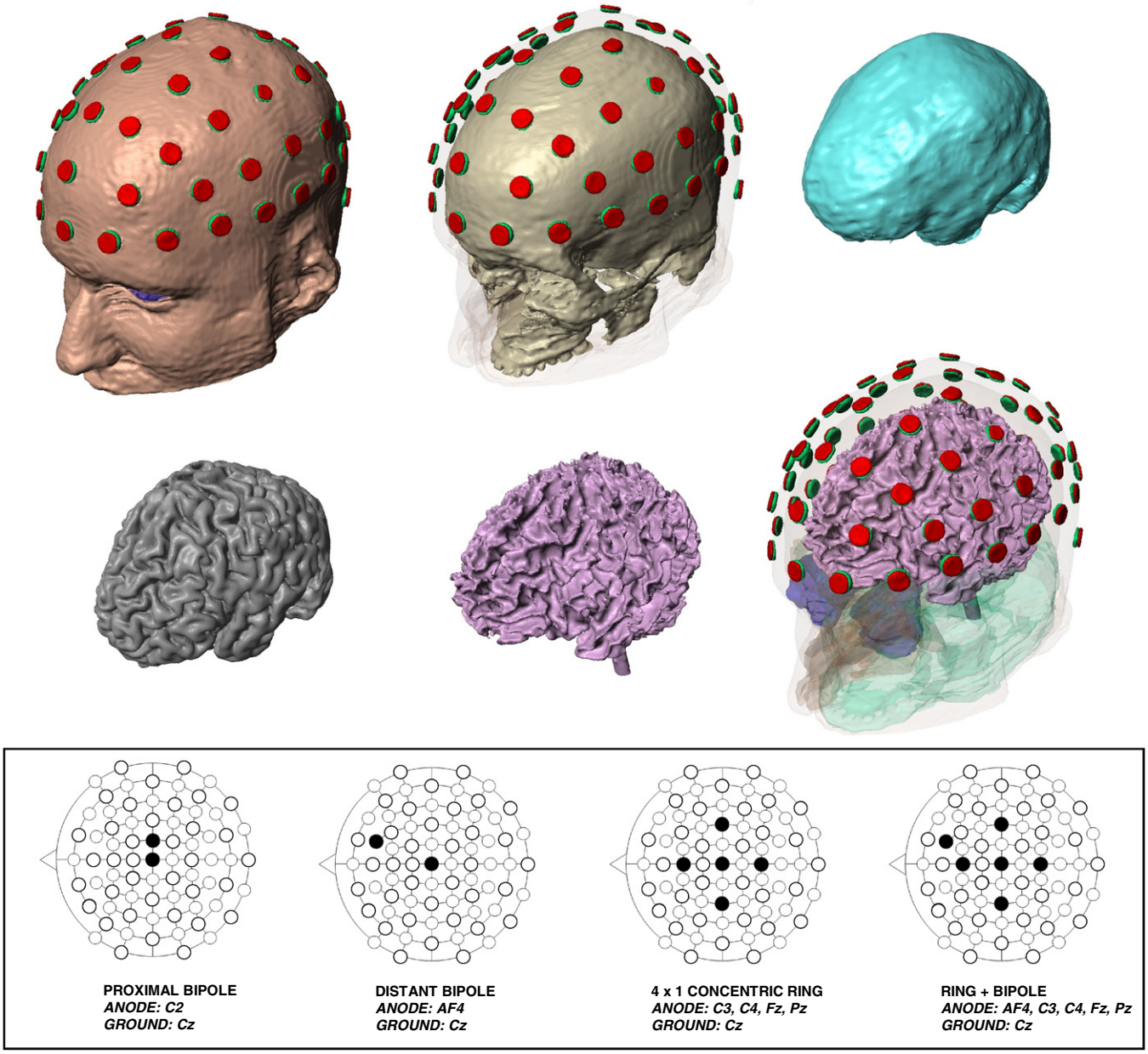

Figure 1. Segmentation masks. Individualized tissue masks of the 34 year old subject used in the study. The top row shows the skin, skull and the CSF masks. The middle row shows the gray matter and white matter masks. The electrode (red) and the gel (green) masks positioned using an automated script is also shown. The bottom row (boxed) shows the electrode placement schematic of the montages tested in the study.

was applied at Cz and all other external surfaces were treated as insulated.

Scalp voltage (V), skull current density (A m^{-2}), and cortical electric field (V m^{-1}) maps for the different electrode montages were determined (figures 3 and 5). EEG analyses typically use 2D circular views (topoplot function) providing the ability to visualize all 64 channel locations at once. To enable direct comparison between the experimental and the modeling approaches, induced scalp potentials on each of the 64 electrodes (barring stimulation electrodes) predicted from the FEM models were also displayed via the topoplot function (EEGLAB) (Delorme and Makeig 2004).

Experimental methods

All experiments were approved by The City College of New York Institutional Review Board. Experiments were performed on the aforementioned 34 year old male subject (also used for individualized brain modeling). The subject was fitted with a conventional EEG cap (BioSemi B.V., Amsterdam, Netherlands) with 64 electrode positions following the 10–10 international system; 2 or 6 positions were fitted with HD stimulation electrodes according to the four electrode configurations modeled (as above), and the remaining positions were used for recording.

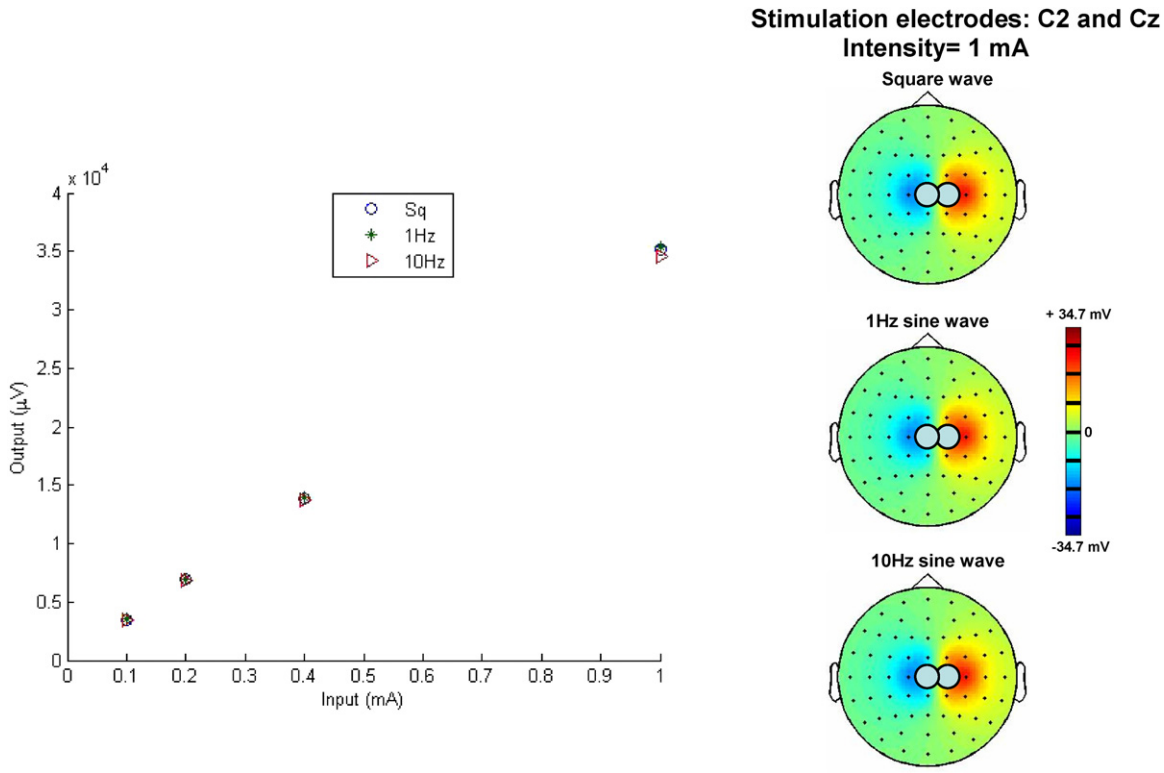

Figure 2. Linearity of scalp voltages induced during transcranial electrical stimulation. The peak induced scalp potential as determined experimentally is plotted as a function of stimulation amplitude and frequency using the proximal bipole montage. The induced scalp potentials are a linear function of stimulation amplitude over the range tested. The spatial map profile was also independent of frequency. The stimulating electrodes on the maps are indicated by closed circles.

Transcranial electrical stimulation. Low-intensity TES was applied using either an analogue isolated current source (Model 2200, A-M Systems, WA) driven by a function generator (Model AFG 320, Tektronix, OR) or stand-alone Soterix 1 × 1 and 4 × 1 stimulators (Soterix Medical, NY). Current was delivered using Ag/AgCl pellet electrodes (A-M Systems, WA) and CCNY-4 gel combination (Minhas *et al* 2010), where the stimulating electrodes replaced recording electrodes in the head-gear according to the stimulation configuration. The Ag/AgCl pellet stimulation electrodes were specifically chosen so as to match the form-factor of the recording Ag/AgCl electrodes. The electrodes were encased in pin-type electrode holders and mounted into the BioSemi headcaps. The holders were fitted with insets from underneath the cap to ensure a gel contact area corresponding to ∼11 mm diameter.

In the first experiment, linearity of scalp voltages with stimulation intensity and frequency was explored using the proximal-bipole montage. 0.1, 0.2, 0.4, and 1 mA current intensity (peak) was used and the resulting scalp voltages measured (see below); for each intensity, monophasic square wave (1 Hz) and monophasic (offset) sine wave (1 or 10 Hz) was used. To minimize skin sensation and avoid irritation while maximizing scalp potential signal-to-noise ratio (S/N), 0.4 mA peak current was used for subsequent experiments. In the second experiment, induced scalp voltage maps were determined for each of the three stimulating electrode configurations. In experiment 3, the spatial linearity of multiple sources was tested by comparing the measured scalp potentials due to the ring + bipole configuration to the 4 × 1 concentric-ring and the distant-bipole configurations independently respectively. A monophasic square wave (1 Hz) *or* monophasic (offset) sine wave (1 or 10 Hz) waveform was typically used for all mapping measurements in experiments 2 and 3. But, as we validated the linearity of induced scalp potentials with current amplitude (figure 2), all results are normalized to per-mA-of-current. Stimulation was applied in repeated exposures of 30 s total duration.

Surface voltage measurements. We used two approaches to measure induced scalp potentials; the two technologies yielded identical results. In one case, scalp potentials were measured sequentially between pairs of electrodes (maintaining a single arbitrary reference) using a custom-made instrumentation amplifier and band-pass filter, with potentials recorded on an oscilloscope. In the second case, scalp potentials were simultaneously measured from all scalp electrodes using the BioSemi EEG (Active Two system, Amsterdam, Netherlands) using packaged acquisition and software analysis. In both cases, scalp potentials were measured using electrodes at multiple locations on the scalp following the 10–10 system—omitting the locations occupied by the stimulating electrodes (though the potential applied to the stimulating electrodes could be measured as the output of the current source, we

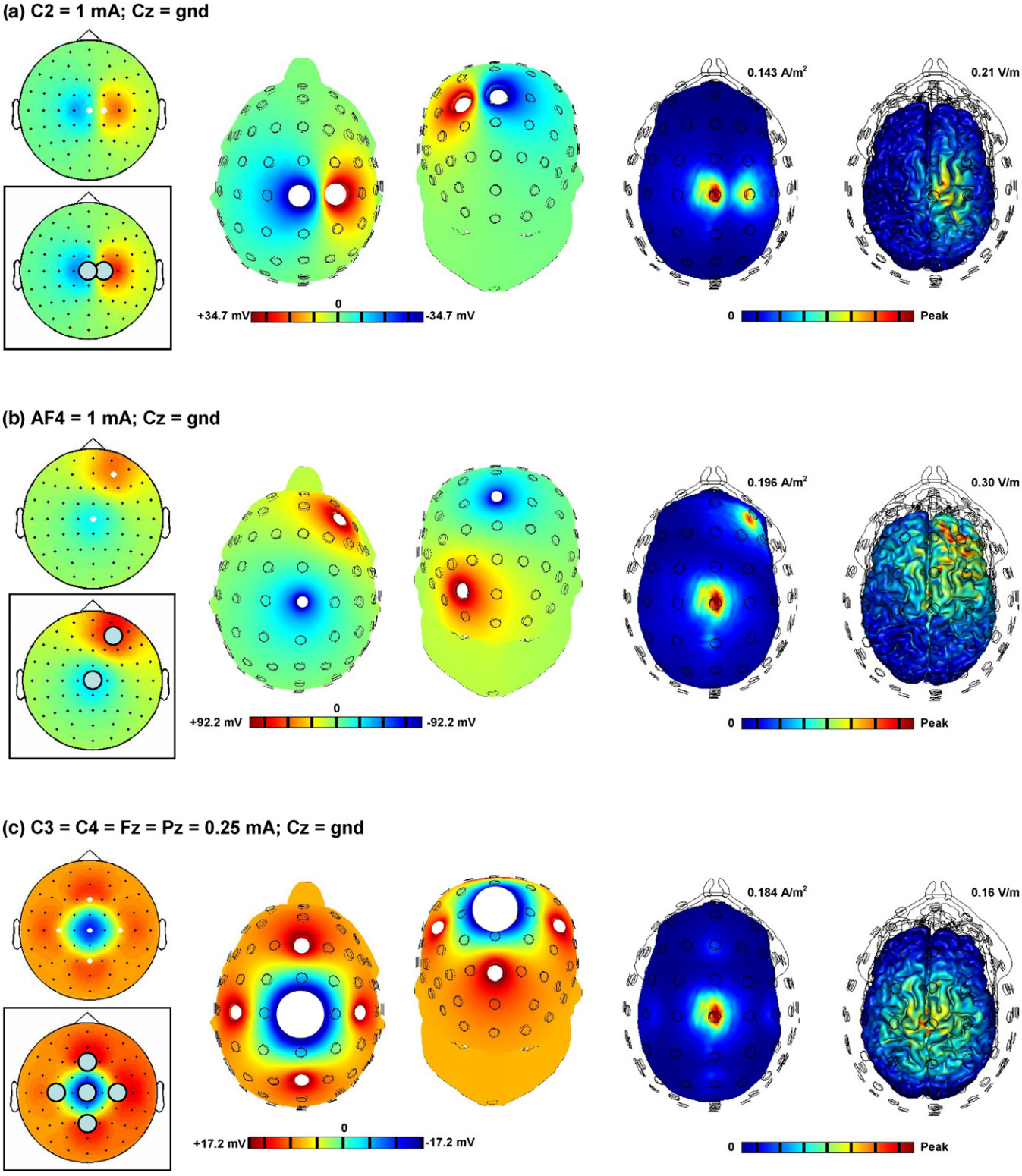

Figure 3. Experimental and FEM model spatial maps of voltage generated on the scalp during transcranial electrical stimulation using three electrode montages. (a) Proximal-bipolar; (b) Distant-bipolar; (c) 4 × 1 concentric ring. The remaining electrodes were used to measure the resulting voltages induced on the scalp. The *boxed* images show the experimental maps. In each case, the current density on the skull and electric field distribution on the gray matter surface as predicted by the model are also shown. The scalp potential maps predicted by the model are rendered in 2D by using topoplot. The stimulating electrodes on the experimental maps are indicated by closed circles.

suspected that because of the electrode interface voltage, this potential did not reflect the voltage at the scalp *under* the stimulation electrodes). The scalp potential distributions are displayed using EEGLAB's topoplot function (see boxed images in figures 3 and 5) and were plotted relative to the approximate middle of the induced voltage range (average

of the minimum and maximum values) thereby producing a symmetric distribution in each plot. For proximal-bipole, voltages were plotted with respect to Iz, which was also the most far-removed location from the stimulation electrodes. For the distant-bipole configuration, location FC2 (approximately mid-way of the distance between stimulation electrodes-AF4 and Cz) was used. For the 4 × 1 concentric-ring, scalp voltages were plotted with respect to the average of the induced voltages at locations FC1, FC2, CP1, and CP2. Location FC2 was used for the ring+ bipole. The spatial profile of skin voltage maps are then compared to the individualized modeling results (based on the person subject to transcranial stimulation) to explore the validity of predictions. Further, the % error difference between the measured and FEM predicted values are reported for each of the configurations tested in experiment 2 (figure 4). It should be noted that the potential maps represented in the figures 3 and 5 depict the voltage distribution when polarity of the ac current is negative at Cz.

Results

The main objective of this study was to characterize scalp potentials induced during TES. In the process we validated the accuracy of a high-resolution individualized FEM forward model of transcranial stimulation by comparing predicted and measured induced scalp voltages. We evaluated four electrode montages to further consider implications for clinical electrode configuration design. As part of this analysis, we explored the temporal and spatial linearity of scalp voltages for low current intensity and frequency.

Linearity of scalp voltages with stimulation current amplitude and waveform

For relatively low frequency and amplitude, we show that scalp voltage amplitude, and by implication tissue current flow, is a linear function of stimulation amplitude. Specifically, the measured peak scalp voltage increases linearly with the applied current (0.1 to 1 mA) between two scalp stimulating electrodes (C2 and Cz); moreover in a frequency independent manner across low-frequencies (square 1 Hz and sine 1 to 10 Hz; figure 2). Similarly, the profile of spatial maps is unchanged across low frequencies. This linearity allows us to normalize spatial maps to per-mA of applied current as well as supports generalizing our results to any stimulation intensity and waveform (e.g. ac) within the linear range.

Spatial maps of scalp voltages during transcranial electrical stimulation and predicted underlying current distribution

We measured the scalp voltages induced during TES using four electrode montages. Results from the experimental measurements were compared to predictions of a high-resolution FEM model—which was individualized to the same subject. Each electrode montage resulted in a distinct surface potential map that was precisely predicted by the subject-specific FEM model (figures 3 and 5). For the proximal-bipole stimulation montage, 1 mA injected current led to 34.7 mV peak measured scalp potential. While the FEM simulation predicted a peak value of 31.1 mV with an error rate of 10.3%. The % error across the recording 10–10 electrodes varied from 4.4% to 13.8% (figure 4). The distant-bipole montage resulted in 92.2 mV peak measured and 77.9 mV peak FEM predicted scalp potential (15.5% error) while the % error varied from 6.9% to 23.8%. The 4 × 1 montage led to 17.2 mV peak measured and 15.1 mV peak model predicted scalp voltage. The % error varied from 5% to 19.6% with an error of 12.2% in the peak values. A higher error % for the distant-bipole than proximal-bipole and the 4 × 1 (both across the overall 10–10 recording array and the peak induced values) is expected as current traverses through a longer intermediate path between the stimulation electrodes. For each electrode montage, the FEM model also predicts the resulting current flow in deeper tissue including the skull current density and the cortical electric fields (figure 3).

Spatial linearity of scalp voltages: multiple stimulation sources

It is expected that when multiple current stimulators are used, the resulting brain electric fields reflect the independent contribution from each source. We verified this assumption at the level of the scalp (figure 5). Specifically we show that stimulating with a six electrode configuration that combines the 4 × 1 configuration and the distant bipolar configuration (with Cz location shared) results in scalp voltages equal to the sum of scalp voltages generated independently by the 4 × 1 and distant-bipolar configurations. The combined six-electrode experimental spatial map is also matched by FEM predictions. The peak measured and predicted scalp potentials are 102.6 and 85.8 mV respectively (16.4 error %). In the discussion we expand on the implications of temporal and spatial linearity for clinical dosage.

Discussion

Linearity in low intensity and frequency transcranial electrical stimulation

For relatively low-intensity and frequency, linearity in TES indicates that: (1) as the applied current intensity increases, the electric field in all regions scales directly with the current amplitude; (2) the induced electric field tracks the waveform of the applied current, independent over the low frequency range tested; as used, for example, in tACS (Antal *et al* 2008, Kanai *et al* 2008) and slow oscillation stimulation (Marshall *et al* 2006). (3) When multiple current sources are used, the resulting electric fields are a summation of the electric fields induced independently by each current source. This linearity is indeed an implicit and ubiquitous assumption in the clinical design of transcranial stimulation protocols—for example when the effects of distinct dosages are compared. Computational forward-models of weak electrical stimulation generally assume linearity and generalize their results (e.g. across waveforms) based on this linearity (Bossetti *et al*

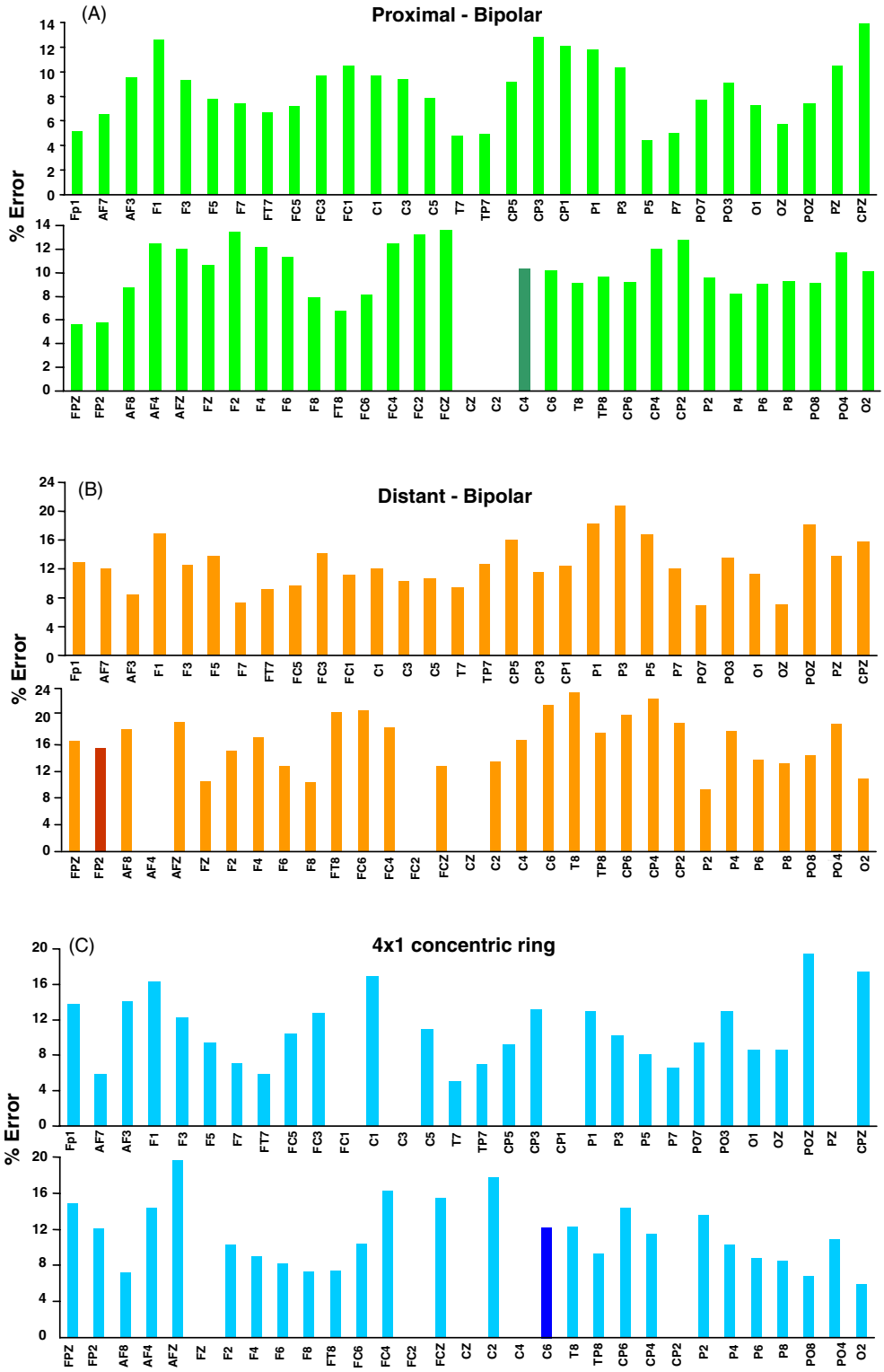

Figure 4. Percentage error between the surface voltage measurements and the FEM model predictions for each of the 10–10 recording array electrodes barring the stimulation and the reference electrodes (see Methods). The error bar at the peak induced location is highlighted in a darker shade for each of the montages.

2008). Moreover, we recently developed an algorithm for optimization of TES leveraging this linearity (Dmochowski *et al* 2011). Here we support this assumption over the intensity and frequency ranges tested.

Scalp and deeper tissue current flow during transcranial electrical stimulation

For all montages, including distant-bipolar, there is current distribution across the entire scalp region between and around

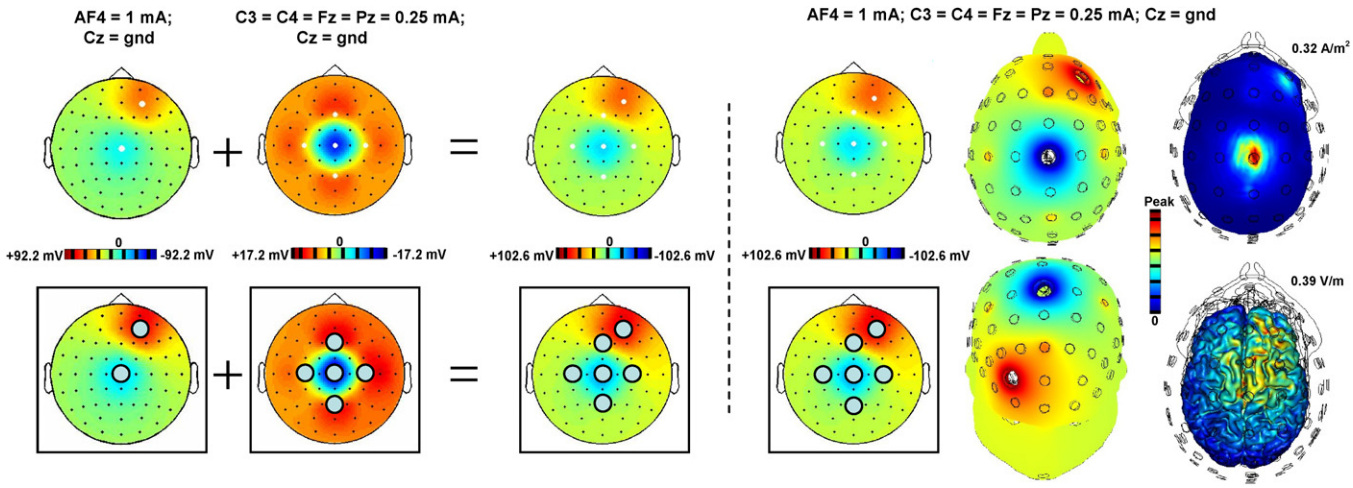

Figure 5. Evaluation of spatial linearity for transcranial electrical stimulation using multiple sources. The scalp voltage induced by a combination montage (ring + distant) equals the summation of the scalp voltages induced by each of the individual montages: ring and distant bipole. This is verified experimentally (boxed images) and by FEM predictions. Stimulating electrodes on the experimental maps are indicated by closed circles. The current density on skull and the electric field on cortical gray matter surface is shown for the combination montage.

electrodes (reflected in a broad scalp voltage distribution). The current density at the skull is however highly localized directly under the stimulation electrodes. Taken together, these two observations imply that though significant current is shunted *tangentially* across the scalp, the currents that crosses *radially* through the skull are restricted to under the stimulation electrodes (i.e. essentially current that is shunted across the scalp has little driving force to cross the skull). Despite focal current entry across the skull, however, the resulting electric fields across the gray matter are still distributed across the cortical entire region between electrodes. This is indeed expected as current entering from one electrode must evidently pass through the *entire* intermediate brain on the way out of the other electrode(s) and the presence of a highly conductive layer of CSF further promotes this broad distribution. We recently proposed that the dogma suggesting skull is a 'low-pass spatial filter' during transcranial electrical flow, diffusing current and severely limiting stimulation focality, was misguided (Datta *et al* 2009). Rather as shown here, the high resistivity of the skull leads to predominantly radial (specifically *undiffused*) current flow. The results of this study provide some experimental support (model validation) and additional insight into this proposed paradigm. Indeed, the highly focalized current flow through the skull is striking given the broad diffusivity in both the superficial skin and underlying gray matter (figure 3).

The degree and extent of current spread has direct implications for the design of electrode montages for effective TES. Using bipolar montages, our model predicts the passage of current through intermediary cortical regions limits the focality of stimulation; use of smaller electrodes does not prevent this (figure 3(b). As expected, the use of more proximal electrodes increases focality (figure 3(a) at the cost of increase scalp shunting (Faria *et al* 2011), which needs to be compensated by increased applied current. The 4 × 1-ring configuration restricts peak current flow to within the 'ring' (figure 3(c)—thus the controllable size of the ring determines the extent of diffusion (Datta *et al* 2008).

Monitoring of scalp voltage during clinical stimulation and relation to safety and electrical impedance tomography

Because scalp voltage reflects the stimulation configuration (electrode montage, current intensity) they provide corroboration that a given clinical dose is being applied correctly. A fault in the stimulation device, a sudden problem with an electrode, or misplaced electrodes, will result in a deviation from an expected scalp voltage map (which is not necessarily evident in electrode resistance or stimulator output voltage); we suggest online monitoring of surface (scalp) voltage (OMSV) may be incorporated as a safety feature in a stimulation device. OMSV can be enhanced by, but does not necessarily require, individualized models. Further translational refinements of OMSV include consideration of template versus subject-specific analysis (Datta *et al* 2012b) and identifying (montage-specific) scalp locations more sensitive to dose changes.

Brain electrical impedance tomography (EIT) involves application of weak transcranial electrical and measurement of resulting scalp voltage changes for the purpose of imaging brain impedance or brain activity (Abascal *et al* 2008, Gilad and Holder 2009, Oh *et al* 2011, Tidswell *et al* 2001). For EIT typically no *a priori* individualized information is used (e.g. MRI scans) and indeed the rationale for EIT is predicated on accurately determining (resolving) individual anatomical or functional differences. Other EIT approaches use anatomical data obtained from independent imaging (e.g. MRI). In contrast to EIT, OMSV returns only a binary decision of 'correct' or 'incorrect' stimulation electrode configuration (placements and faults). OMSV can still leverage the sophistication of analysis tools developed for EIT, especially in the absence of MRI based subject-specific

modeling. Recent work in EIT includes: (1) exploration of commercially available FE tools to build accurate meshes with the goal of improving image reconstruction (Bayford *et al* 2001); (2) incorporation of tissue anisotropy (Abascal *et al* 2008); (3) rapid generation of patient-specific meshes (Vonach *et al* 2012); (4) innovative stimulation electrode design (Gilad *et al* 2007) and (5) approaches to inform specification and optimal electrode placement using EIT as well as magnetic detection EIT (Gilad *et al* 2009).

All of these advances made for EIT need to be further explored in the realm of transcranial stimulation approaches. While the goal of TES models remains geared towards optimizing and understanding clinical dose, the technical similarity of the two approaches allow incorporation of developments made in one field into the other. The advances made in patient-specific gyri-sulci precise transcranial modeling could thus be potentially leveraged for EIT as well (Datta *et al* 2011, 2012b, Halko *et al* 2011, Bikson *et al* 2012).

Accuracy of FEM models of transcranial electrical stimulation

Indeed, significant engineering effort has recently been directed toward increasing the sophistication of FEM simulation tools (Wagner *et al* 2007, Sadleir *et al* 2010, Salvador *et al* 2010, Parazzini *et al* 2011, Datta *et al* 2011, Dasilva *et al* 2012, Im *et al* 2012). FEM forward models of transcranial stimulation are the primary basis for considering how the choice of electrode montage effects resulting current flow through the brain, and hence the targeting of neuromodulation. Yet there remains a dearth of experimental validation of these models—and increased model sophistication and precision does not equate with accuracy (Bikson and Datta 2012). In this paper we validated the accuracy of a high-resolution subject-specific FEM model by measuring scalp voltages. As discussed above, a predictive forward model may indicate changes as to how electrode montage is currently considered in clinical practice, as well as methodologies to optimize targeting.

Our measurements of induced scalp voltages support the accuracy of the high-resolution individualized FEM model used in this study, but does not directly validate the model prediction of *brain* current flow. Still, the consistency of modeling predictions with experimental data supports model validity and these scalp voltage measurements can be used to falsify inaccurate models. More generally, our approach provides the first direct basis for comparing the accuracy of the broad range of modeling approaches under development (Datta *et al* 2011, Halko *et al* 2011, Parazzini *et al* 2011, Suh *et al* 2010, Windhoff *et al* 2011). Specifically, measured scalp voltage values can be compared to predicted potential values. The basis of the mismatch reported in this study can be further explored in future studies by selecting among alternative models (e.g. manual correction, DTI calibration approaches) and adjusting model parameters (tissue conductivities). Furthermore, future work should explore multiple subjects by comparing predicted and measured scalp potentials to address both the value of individualized modeling and subject-to-subject variability (Datta *et al* 2012b).

References

Abascal J F *et al* 2008 Use of anisotropic modelling in electrical impedance tomography: description of method and preliminary assessment of utility in imaging brain function in the adult human head *Neuroimage* **43** 258–68

Antal A, Boros K, Poreisz C, Chaieb L, Terney D and Paulus W 2008 Comparatively weak after-effects of transcranial alternating current stimulation (tACS) on cortical excitability in humans *Brain Stimul.* **1** 97–105

Antal A *et al* 2012 Imaging artifacts induced by electrical stimulation during conventional FMRI of the brain *Neuroimage*

Bayford R H, Gibson A, Tizzard A, Tidswell T and Holder D S 2001 Solving the forward problem in electrical impedance tomography for the human head using IDEAS (integrated design engineering analysis software), a finite element modelling tool *Physiol. Meas.* **22** 55–64

Bikson M and Datta A 2012 Guidelines for precise and accurate computational models of tDCS *Brain Stimul.* **5** 430–1

Bikson M, Datta A, Rahman A and Scaturro J 2010 Electrode montages for tDCS and weak transcranial electrical stimulation: role of 'return' electrode's position and size *Clin. Neurophysiol.* **121** 1976–8

Bikson M, Rahman A, Datta A, Fregni F and Merabet L 2012 High-resolution modeling assisted design of customized and individualized transcranial direct current stimulation protocols *Neuromodulation* **15** 306–15

Borckardt J J *et al* 2012 A pilot study of the tolerability and effects of high-definition transcranial direct current stimulation (HD-tDCS) on pain perception *J. Pain* **13** 112–20

Bossetti C A, Birdno M J and Grill W M 2008 Analysis of the quasi-static approximation for calculating potentials generated by neural stimulation *J. Neural Eng.* **5** 44–53

Calancie B, Harris W, Broton J G, Alexeeva N and Green B A 1998 Threshold-level multipulse transcranial electrical stimulation of motor cortex for intraoperative monitoring of spinal motor tracts: description of method and comparison to somatosensory evoked potential monitoring *J. Neurosurg.* **88** 457–70

Dasilva A F *et al* 2012 tDCS-induced analgesia and electrical fields in pain-related neural networks in chronic migraine *Headache*

Datta A, Baker J M, Bikson M and Fridriksson J 2011 Individualized model predicts brain current flow during transcranial direct-current stimulation treatment in responsive stroke patient *Brain Stimul.* **4** 169–74

Datta A, Bansal V, Diaz J, Patel J, Reato D and Bikson M 2009 Gyri-precise head model of transcranial direct current stimulation: improved spatial focality using a ring electrode versus conventional rectangular pad *Brain Stimul.* **2** 201–7

Datta A, Dmochowski J P, Guleyupoglu B, Bikson M and Fregni F 2012a Cranial electrotherapy stimulation and transcranial pulsed current stimulation: a computer based high-resolution modeling study *Neuroimage*

Datta A, Elwassif M, Battaglia F and Bikson M 2008 Transcranial current stimulation focality using disc and ring electrode configurations: FEM analysis *J. Neural Eng.* **5** 163–74

Datta A, Truong D, Minhas P, Parra L C and Bikson M 2012b Inter-individual variation during transcranial direct current stimulation and normalization of dose using MRI-derived computational models *Front. Psychiatry* **3** 91

Delorme A and Makeig S 2004 EEGLAB: an open source toolbox for analysis of single-trial EEG dynamics *J. Neurosci. Methods* **134** 9–21

Dmochowski J P, Datta A, Bikson M, Su Y and Parra L C 2011 Optimized multi-electrode stimulation increases focality and intensity at target *J. Neural Eng.* **8** 046011

Dymond A M, Coger R W and Serafetinides E A 1975 Intracerebral current levels in man during electrosleep therapy *Biol. Psychiatry* **10** 101–4

Faria P, Hallett M and Miranda PC 2011 A finite element analysis of the effect of electrode area and inter-electrode distance on the spatial distribution of the current density in tDCS *J. Neural Eng.* **8** 066017

Ferdjallah M, Bostick F X Jr and Barr R E 1996 Potential and current density distributions of cranial electrotherapy stimulation (CES) in a four-concentric-spheres model *IEEE Trans. Biomed. Eng.* **43** 939–43

Fregni F *et al* 2005 Anodal transcranial direct current stimulation of prefrontal cortex enhances working memory *Exp. Brain Res.* **166** 23–30

Gilad O and Holder D S 2009 Impedance changes recorded with scalp electrodes during visual evoked responses: implications for electrical impedance tomography of fast neural activity *Neuroimage* **47** 514–22

Gilad O, Horesh L and Holder D S 2007 Design of electrodes and current limits for low frequency electrical impedance tomography of the brain *Med. Biol. Eng. Comput.* **45** 621–33

Gilad O, Horesh L and Holder D S 2009 A modelling study to inform specification and optimal electrode placement for imaging of neuronal depolarization during visual evoked responses by electrical and magnetic detection impedance tomography *Physiol. Meas.* **30** S201–24

Halko M A, Datta A, Plow E B, Scaturro J, Bikson M and Merabet L B 2011 Neuroplastic changes following rehabilitative training correlate with regional electrical field induced with tDCS *Neuroimage* **57** 885–91

Im C H, Park J H, Shim M, Chang W H and Kim Y H 2012 Evaluation of local electric fields generated by transcranial direct current stimulation with an extracephalic reference electrode based on realistic 3D body modeling *Phys. Med. Biol.* **57** 2137–50

Kanai R, Chaieb L, Antal A, Walsh V and Paulus W 2008 Frequency-dependent electrical stimulation of the visual cortex *Curr. Biol.* **18** 1839–43

Lisanby S H 2007 Electroconvulsive therapy for depression *New Engl. J. Med.* **357** 1939–45

Marshall L, Helgadottir H, Molle M and Born J 2006 Boosting slow oscillations during sleep potentiates memory *Nature* **444** 610–3

Mendonca M E *et al* 2011 Transcranial DC stimulation in fibromyalgia: Optimized cortical target supported by high-resolution computational models *J. Pain* **12** 610–7

Minhas P *et al* 2010 Electrodes for high-definition transcutaneous DC stimulation for applications in drug delivery and electrotherapy, including tDCS *J. Neurosci. Methods* **190** 188–97

Miranda P C, Lomarev M and Hallett M 2006 Modeling the current distribution during transcranial direct current stimulation *Clin. Neurophysiol.* **117** 1623–9

Nitsche M A and Paulus W 2000 Excitability changes induced in the human motor cortex by weak transcranial direct current stimulation *J. Physiol.* **527** 633–39

Oh T, Gilad O, Ghosh A, Schuettler M and Holder D S 2011 A novel method for recording neuronal depolarization with recording at 125–825 Hz: implications for imaging fast neural activity in the brain with electrical impedance tomography *Med. Biol. Eng. Comput.* **49** 593–604

Parazzini M, Fiocchi S, Rossi E, Paglialonga A and Ravazzani P 2011 Transcranial direct current stimulation: estimation of the electric field and of the current density in an anatomical human head model *IEEE Trans. Biomed. Eng.* **58** 1773–80

Rothwell J, Burke D, Hicks R, Stephen J, Woodforth I and Crawford M 1994 Transcranial electrical stimulation of the motor cortex in man: further evidence for the site of activation *J. Physiol.* **481** 243–50

Rush S and Driscoll D A 1968 Current distribution in the brain from surface electrodes *Anesth. Analg.* **47** 717–23

Sadleir R J, Vannorsdall T D, Schretlen D J and Gordon B 2010 Transcranial direct current stimulation (tDCS) in a realistic head model *Neuroimage* **51** 1310–8

Salvador R, Mekonnen A, Ruffini G and Miranda P C 2010 Modeling the electric field induced in a high resolution head model during transcranial current stimulation *Proc. Annu. Conf. of IEEE Engineering in Medicine and Biology Society* vol 2010 pp 2073–6

Saypol J M, Roth B J, Cohen L G and Hallett M 1991 A theoretical comparison of electric and magnetic stimulation of the brain *Ann. Biomed. Eng.* **19** 317–28

Schroeder M J and Barr R E 2001 Quantitative analysis of the electroencephalogram during cranial electrotherapy stimulation *Clin. Neurophysiol.* **112** 2075–83

Smith S M 2002 Fast robust automated brain extraction *Hum. Brain Mapp.* **17** 143–55

Stecker M M 2005 Transcranial electric stimulation of motor pathways: a theoretical analysis *Comput. Biol. Med.* **35** 133–55

Suh H S, Lee W H, Cho Y S, Kim J H and Kim T S 2010 Reduced spatial focality of electrical field in tDCS with ring electrodes due to tissue anisotropy *Proc. Annu. Conf. of IEEE Engineering in Medicine and Biology Society* vol 2010 pp 2053–6

Tidswell T, Gibson A, Bayford R H and Holder D S 2001 Three-dimensional electrical impedance tomography of human brain activity *Neuroimage* **13** 283–94

Vonach M *et al* 2012 A method for rapid production of subject specific finite element meshes for electrical impedance tomography of the human head *Physiol. Meas.* **33** 801–16

Wagner T, Fregni F, Fecteau S, Grodzinsky A, Zahn M and Pascual-Leone A 2007 Transcranial direct current stimulation: a computer-based human model study *Neuroimage* **35** 1113–24

Windhoff M, Opitz A and Thielscher A 2011 Electric field calculations in brain stimulation based on finite elements: an optimized processing pipeline for the generation and usage of accurate individual head models *Hum. Brain Mapp.*

Zhang Y, Brady M and Smith S 2001 Segmentation of brain MR images through a hidden Markov random field model and the expectation-maximization algorithm *IEEE Trans. Med. Imaging* **20** 45–57

QUERIES

Page 1

Q1

Author: Please be aware that the color figures in this article will only appear in color in the Web version. If you require color in the printed journal and have not previously arranged it, please contact the Production Editor now.

Page 9

Q2

Author: Please check the details for any journal references that do not have a blue link as they may contain some incorrect information. Pale purple links are used for references to arXiv e-prints.

Q3

Author: Please provide the volume and page numbers in references 'Antal *et al* (2012)', 'Dasilva (2012)', 'Datta *et al* (2012a)' and 'Windhoff *et al* (2011)'.